Proceedings of the 21st ICSMGE, Vienna, Austria, 14 – 19 June 2026. Pistrol, Adam & Schweiger (eds.)
Published by: ÖGG, Austrian Society for Geomechanics, Salzburg, Austria, ISBN 978-3-9503898-4-5
https://doi.org/10.53243/ICSMGE2026-114

Justification of an improved soil base model for buildings of different storeys

Oleksandr Samorodov, Sergii Tabachnikov, Svitlana Yesakova, **Oleh Krotov**
Department of Geotechnics, Underground Structures and Hydrotechnical Construction, O.M. Beketov National University of Urban Economy in Kharkiv, Kharkiv, Ukraine, s.v.tabachnikov@ukr.net

ABSTRACT: Problem Statement. In the construction of multi-storey and high-rise buildings subjected to substantial foundation loads - particularly when weak, water-saturated soils are present near the surface - pile-raft foundations are widely implemented to comply with deformation limits set by building regulations (DBN V.2.1-10:2018, 2018). However, the use of raft foundations in such conditions must be validated through engineering analyses supported by a scientifically substantiated soil base model and its corresponding parameters. This paper proposes an improved soil base model conceptualized as a continuous "stepped" layer with limited load distribution capacity. The justification of this model is based on a comparison of numerical simulation outcomes with real settlement data obtained from two adjacent multi-storey buildings constructed on raft foundations. Findings. The numerical modeling was carried out for the raft foundations of a two-section building characterized by varying floor heights across sections. The simulation addressed the interaction within the soil–foundation–structure system, incorporating the proposed “stepped” soil layer model with distinct deformation behaviors across layers. The results support the model’s validity for analyzing the deformation behavior of buildings with sectionally different storey numbers situated on extensive raft foundations above shallow soft sandy soils. The inclusion of compressible layer thickness variations and the application of the "Hardening Soil" constitutive law in the improved model enhance the precision of simulating horizontal displacements (tilts) between structural sections.

KEYWORDS: raft foundation, soil base model, compressible layer, model improvement, field monitoring, settlement analysis, tilt.

1 INTRODUCTION

Since the mid-20th century, engineering practice has extensively employed a simplified analytical model of the soil base, represented as a linear continuous layer, to perform foundation calculations. This approach, enshrined in national design standards-including those currently in force (Samorodov and Tabachnikov, 2023) requires only the definition of the compressible layer thickness H and two key mechanical parameters: the deformation modulus E and Poisson’s ratio ν. However, this classical formulation lacks spatial confinement in the horizontal plane, which limits its applicability in more refined three-dimensional simulations.

The increasing availability of high-performance numerical tools (such as SOFiSTiK, ABAQUS, Plaxis, SCAD, and Lira) has enabled more advanced modeling of the soil–foundation–structure interaction. In these platforms, the soil base is frequently represented as a continuous layer with finite load-distribution capability (Figure 1), which incorporates not only vertical constraints at a prescribed depth H but also horizontal limitations defined over a finite area B × L (Empfehlungen des Arbeitskreises, 2014; Wani and Showkat, 2018; Briaud, 2013; Nosenko, 2012; Nosenko and Krivenko, 2020; Skochko and Shabaltun, 2020; Ter-Martirosyan and Ter-Martirosyan, 2009; Braja, 2017; Samorodov and Tabachnikov, 2024).

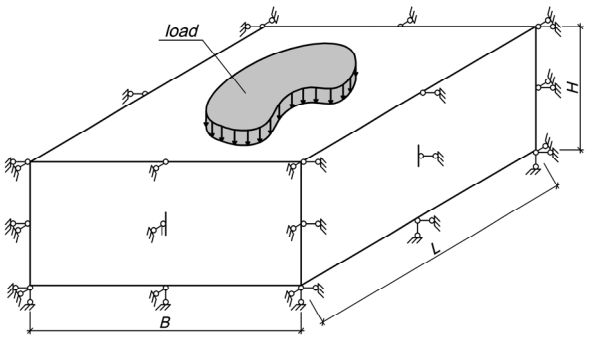

Figure 1. Soil base model as a continuous layer with finite distribution capability (three-dimensional case).

These boundary conditions stem from the physical observation that external loads induce a spatially bounded stress–strain zone within the soil. Beyond this zone, deformations become negligible due to the insignificant magnitude of additional stresses at the soil mass periphery (Braja, 2017; Kushner, 2008; Vynnykov 2005). Furthermore, the model allows for assigning custom-defined strain laws, including time-dependent behavior, enabling better alignment with observed soil response characteristics. Under plane strain conditions, this concept simplifies to a two-dimensional formulation the well-established model of a finite-width continuous layer (Luchkovsky, 2020).

2 RESEARCH MATERIALS AND METHODS

This study introduces an enhanced soil base model described as a continuous stepped layer of finite distribution capability (CSLFDC), which enables a more accurate representation of the interaction between large-area foundations of adjacent buildings with differing numbers of storeys (Samorodov and Tabachnikov, 2023; Samorodov, 2024). The CSLFDC model incorporates the physical and mechanical characteristics of the soil, the geometric configuration of its layers in relation to their deformation and load distribution potential and accommodates diverse boundary conditions required for numerical analysis of the soil–foundation–structure system. A key distinguishing feature of this model lies in its lower boundary, which follows a stepped geometry, reflecting variations in the thickness of compressible soil layers beneath each foundation of the buildings.

Figure 2 presents an illustrative example of constructing the stepped lower boundary of the improved soil base model (1), which incorporates the physical and mechanical properties of subsoil layers as well as their load distribution capability, characterized by the distribution angle α (Empfehlungen des Arbeitskreises, 2014). The model reflects the varying thicknesses of compressible layers (active deformation zones) $H_{p,i}$ located beneath each foundation of width b_i, which transfers the corresponding load p_i to the base.

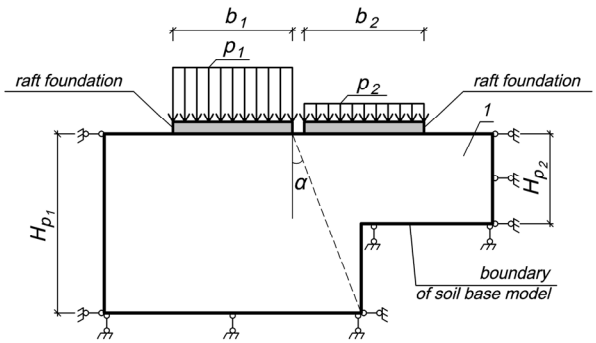

Figure 2. Example of constructing the lower boundary of the improved soil base model in the form of CSLFDC.

The subject of this study is the deformation behavior of the soil base beneath the raft foundations of adjacent sixteen-storey residential buildings, which include underground and mechanical floors. The construction site is situated in Kharkiv, Ukraine, Osnovianskyi district, at 2B Lisavetinska Street. The general layout of the buildings, including the analyzed structure (Building 7, Sections 1 and 2), is presented in Figure 3.

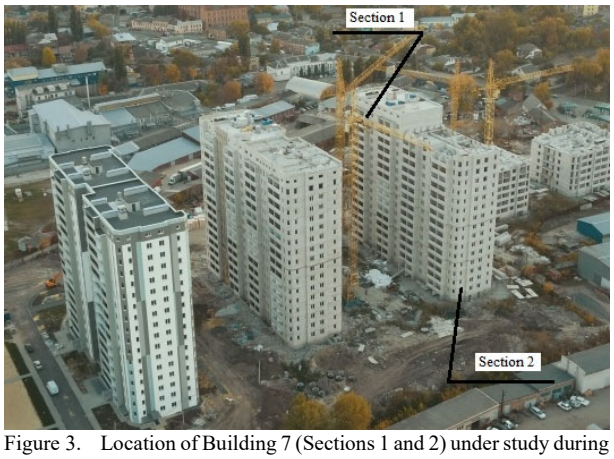

Figure 3. Location of Building 7 (Sections 1 and 2) under study during construction.

The two sections of the building exhibit a symmetrical layout, with each section representing a mirror image of the adjacent one in plan. The structural concept follows a frameless system. Reinforced concrete hollow-core slabs are employed as the main load-bearing elements for the structural floors. The overall spatial stiffness of the building is provided by the interaction between the horizontal and vertical load-bearing components.

The primary load-bearing elements of the buildings are:

- Brick walls constructed from silica brick with thicknesses of 150, 250, 380, and 510 mm.
- Prefabricated floor structures consisting of 220 mm thick reinforced concrete hollow-core slabs.\
- Prefabricated basement walls composed of 500 mm thick concrete blocks.

The geological profile at the project site, extending to a depth of 20.0 m, consists predominantly of Neogene–Quaternary sediments, including alluvial and deluvial loams and sands, overlain by a shallow layer of fill material. At greater depths, greenish-grey and bluish-grey clays and greenish sandstones of the Upper Paleogene are encountered, underlain by clays of the Kyiv Subformation and Middle Paleogene sandstones.

The hydrogeological conditions are defined by a low-pressure Quaternary alluvial aquifer. During the site investigation in June 2020, the groundwater table was observed at depths ranging from 1.8 to 3.3 m, corresponding to absolute elevations of 101.51 to 102.92 m. The site is classified as flood-prone. During periods of high precipitation and spring flooding, groundwater levels may rise significantly, approaching the surface.

The layout of the boreholes is shown in Figure 4.

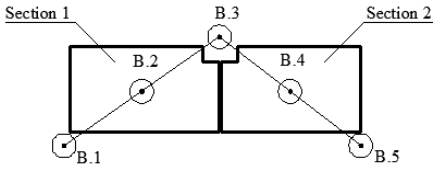

Figure 4. Borehole layout.

An engineering-geological cross-section illustrating the approximate position of the foundation slabs is presented in Figure 5.

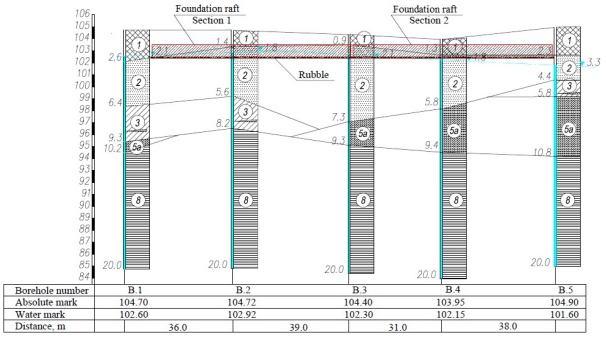

Figure 5. Engineering and geological section 1-5.

The soil description and their properties are summarized in Table 1.

Table 1. Soil types and descriptions.

Symbol	EGE-1	EGE-2	EGE-3	EGE-5a	EGE-8
γ	-	18.88	19.40	20.23	16.74
γ_{sat}	-	19.45	19.60	19.22	16.88
γ_s	-	26.09	26.68	20.15	26.74
γ_{sb}	-	9.97	9.99	10.65	7.47
W	-	0.19	0.22	0.19	0.38
e	-	0.63	0.68	0.54	1.06
c	-	2	23	4	37
φ	-	33	18	36	17
E	-	28(9*)	15	38	13
I_L	-	-	0.60	-	0.24
I_P	-	-	0.11	-	0.28

* - the value was obtained according to the plate bearing tests

The parameters considered in the analysis include:

- Specific weight of soil (γ, kN/m³).
- Specific weight of water-saturated soil (γ_{sat}, kN/m³).
- Specific weight of soil fragments (γ_s, kN/m³).
- Specific weight of soil suspended in water (γ_{sb}, kN/m³).
- Natural moisture content (W, unit).
- Porosity coefficient (e, unit).
- Specific soil adhesion (c, kPa).
- Angle of internal friction (φ, degrees).
- Modulus of deformation in the natural / water-saturated state (E, MPa).
- Liquid limit (I_L, unit).
- Plasticity (I_P, unit).

The foundations of the residential buildings are designed as reinforced concrete slabs with a thickness of 1000 mm, with their bottom elevation set at an absolute level of 102.80 m. The subgrade beneath the foundations consists of EGE-2 fine-grained sands, exhibiting varying degrees of water saturation and medium density.

The maximum average pressure beneath the foundation slab, resulting solely from the dead load of the erected structures and without the application of load amplification factors, does not exceed the calculated bearing resistance of the subsoil: $p = 230.02$ kPa < $R = 388.0$ kPa.

3 SIMULATION OF THE BASE–FOUNDATIONS–BUILDINGS SYSTEM AND CALCULATION RESULTS

To evaluate the influence of the improved soil base model, a finite element model of the base-foundation-structure system was developed using the PLAXIS 3D software suite. The model comprises the soil base and a two-section, 17-storey building supported by raft foundations.

The structural elements of the building including the foundation raft, foundation block walls, brick walls, and floor slabs - were modeled using plate finite elements with an elastic material model. All materials were assumed to be nonporous. The geometric and mechanical characteristics of these structural components, including thickness (d), specific weight (γ), modulus of elasticity (E), and Poisson's ratio (ν), are presented in Table 2. The soil base was modeled as a continuous stepped layer of finite distribution capability (CSLFDC) using solid finite elements. The assigned physical and mechanical properties correspond to the actual engineering and geological conditions of the construction site, as detailed in Figure 5 and Table 1. The thickness of the modeled soil layer was constrained by the depth of the compressible zone corresponding to each stage of loading imposed by the erected building volume.

Table 2. Parameters of building structures.

Structural Element	d (m)	γ (kN/m³)	E (kN/m²)	ν (units)
Foundation raft	1.0	25.0	$30.0 \cdot 10^6$	0.2
Foundation block wall	0.5	25.0	$30.0 \cdot 10^6$	0.25
Brick wall	0.15 / 0.25 / 0.38 / 0.51	19.0	$3.2 \cdot 10^6$	0.25
Floor slab	0,14	25.0	$30.0 \cdot 10^6$	0.2

Three principal constitutive models were employed to simulate soil behavior (PLAXIS CONNECT Edition V20, 2020): the Linear Elastic (LE) model, the Mohr-Coulomb (MC) model, and the Hardening Soil (HS) model, an elastoplastic formulation incorporating stress-dependent soil stiffness.

The principal input parameters of the soil base used for each of the three selected constitutive models are summarized in Table 3.

Linear Elastic (LE) model. The linear elastic model is governed by Hooke's law for isotropic materials. It requires only two primary input parameters: Young's modulus (E, kN/m²) and Poisson's ratio (v, unit). The specific weight of soil (γ, kN/m³) was also included to establish the initial stress state in the soil base, taking into account the hydrogeological conditions of the site.

Mohr-Coulomb (MC) model. This elastic–perfectly plastic model is defined by five input parameters: the deformation characteristics (E, kN/m² and v, unit), the shear strength parameters (internal friction angle φ, ° and cohesion c, kN/m²), and the dilatancy angle (ψ, °).

Table 3. Main parameters adopted for the soil base in different constitutive models.

EGE Number	Linear Elastic (LE)	Mohr-Coulomb (MC)	Hardening Soil (HS)
EGE-2	E'=9000 kN/m² v'=0.3	E'=9000 kN/m² v'=0.3 c'_{ref}=2 kN/m² φ'=33°; ψ=3° e_{init}=0.63	E_{50}^{ref}=9000 kN/m² E_{oed}^{ref}=9000 kN/m² E_{ur}^{ref}=27000 kN/m² c'_{ref}=2 kN/m² φ'=33°; ψ=3°; e_{init}=0.63
EGE-3	E'=15000 kN/m² v'=0.35	E'=15000 kN/m² v'=0.35 c'_{ref}=23 kN/m² φ'=18°; ψ=0° e_{init}=0.68	E_{50}^{ref}=15000 kN/m² E_{oed}^{ref}=15000 kN/m² E_{ur}^{ref}=45000 kN/m² c'_{ref}=23 kN/m² φ'=18°; ψ=0°; e_{init}=0.68
EGE-5a	E'=38000 kN/m² v'=0.3	E'=38000 kN/m² v'=0.3 c'_{ref}=4 kN/m² φ'=36°; ψ=6° e_{init}=0.54	E_{50}^{ref}=38000 kN/m² E_{oed}^{ref}=38000 kN/m² E_{ur}^{ref}=114000 kN/m² c'_{ref}=4 kN/m² φ'=36°; ψ=6°; e_{init}=0.54
EGE-8	E'=13000 kN/m² v'=0.4	E'=13000 kN/m² v'=0.4 c'_{ref}=37 kN/m² φ'=17°; ψ=0° e_{init}=1.06	E_{50}^{ref}=13000 kN/m² E_{oed}^{ref}=13000 kN/m² E_{ur}^{ref}=39000 kN/m² c'_{ref}=37 kN/m² φ'=17°; ψ=0°; e_{init}=1.06

Hardening Soil (HS) model. Similar to the Mohr-Coulomb model, the HS model defines the ultimate stress state using φ (°), c (kN/m²), and ψ (°). However, soil stiffness is described through three separate moduli: E_{50} (secant stiffness in a triaxial test, kN/m²), $E_{(ur)}$ (unloading/reloading stiffness, kN/m²), and $E_{oe}d$ (oedometric stiffness, kN/m²). Default relationships are typically applied: $E_{(ur)} \approx 3E_{50}$ and $E_{oed} \approx E_{50}$. Unlike the Mohr-Coulomb model, the HS model accounts for stress-dependent stiffness, where all stiffness moduli increase with confining pressure. These values are defined relative to a reference stress, conventionally taken as 100 kPa.

The applied loading includes the self-weight of all load-bearing and enclosing structural components. According to the calculations (DBN V.2.1-10:2018; Samorodov, 2017), and without applying the recommended minimum thickness values, the depth of the compressible soil layer H_c was determined based on the average pressure p_{av} beneath the foundation slab at various stages of structural erection. At $p_{av} = 24.95$ kPa, corresponding to the dead load during basement construction, H_c is taken as 2.0 m. As the number of constructed floors increases, the corresponding values are as follows: $H_c = 9.5$ m at $p_{av} = 65.21$ kPa (three floors erected, $n = 3$); $H_c = 10.5$ m at $p_{av} = 98.55$ kPa ($n = 6$); $H_c = 11.0$ m at $p_{av} = 120.40$ kPa ($n = 8$); $H_c = 13.5$ m at $p_{av} = 153.21$ kPa ($n = 11$); $H_c = 16.0$ m at $p_{av} = 191.60$ kPa ($n = 14$); and $H_c = 18.0$ m at $p_{av} = 230.02$ kPa ($n = 17$).

In the first stage, numerical analysis was conducted to evaluate the stress–strain behavior of the base–foundations–buildings system using a CSLFDC-type soil base model with a uniform maximum compressible layer thickness, as illustrated in Figure 1. The model boundaries were defined both vertically and horizontally by a distance equal to the maximum depth of the compressible zone, $H_c = 18.0$ m, corresponding to the fully loaded condition. The distribution of compressive stresses in depth was assumed to occur at an angle $\alpha = 45°$ from the vertical, measured from the edges of the loaded foundations (Empfehlungen des Arbeitskreises, 2018). At subsequent

construction stages, the thickness of the compressible layer was adjusted to reflect the actual stress increment from the progressive erection of the building volume.

To account for the variation in compressible layer thickness (active deformation zone) beneath the foundations during progressive loading on the soil base, a simplified modeling approach was adopted. In this method, an underlying layer composed of an almost rigid, non-deformable material with a high modulus of elasticity ($E = 100.0 \times 10^9$ kN/m²) was introduced below the calculated lower boundary of the most heavily loaded section, corresponding to the number of erected floors (Figure 6).

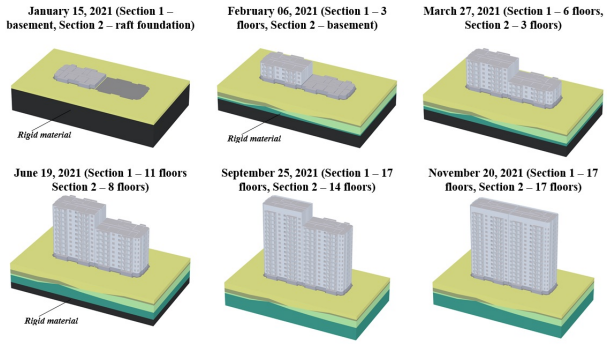

Figure 6. Calculation scheme of the model at the first stage of analysis with a uniform compressible layer based on observation dates and the number of erected floors.

Using the defined model parameters and initial data, the interaction between the structure and the improved soil base model was simulated. The analysis was performed using the finite element method, providing absolute values of the stress–strain state for the system. Time-dependent behavior was not considered in this simulation.

At the second stage, numerical calculations were carried out for the base–foundations–buildings system incorporating a stepped compressible layer within the CSLFDC soil model. This approach accounted for variation in compressible layer depth beneath each foundation, depending on the applied load, and incorporated the assumed stress distribution angle α, as shown in Figure 2 and Figure 3.

The vertical boundaries (in depth) were defined individually for each foundation section, corresponding to the calculated thickness H_i of the compressible layer under varying load conditions. To represent the active deformation zones, the depth spread of compressive stresses was assumed to propagate at an angle of approximately $\alpha = 25°$ from the vertical, measured from the inner edge of the most heavily loaded foundation (Samorodov et al., 2024). The horizontal (in-plane) boundaries, as in the first stage of the study, were set at a distance equal to the maximum compressible layer thickness of $H = 18.0$ m, corresponding to the full loading scenario.

During construction of the stepped lower boundary of the soil base model, which reflects the variation in compressible layer thicknesses, a nearly rigid, non-deformable material with a high modulus of elasticity ($E = 100.0 \times 10^9$ kN/m²) was applied beneath the active zones (Figure 7).

To analyze the simulation results and compare them with field observations, control points in the finite element model were placed at the same locations as the benchmarks on the actual two-section building. Additional benchmarks were also distributed along the height of each section. Based on the numerical outcomes, the deformation behavior of each section was evaluated with respect to the load distribution, the adopted soil base model, and the selected constitutive model for soil behavior. The computed settlement values were subsequently used in comparison with the measured settlement data recorded during the building's construction.

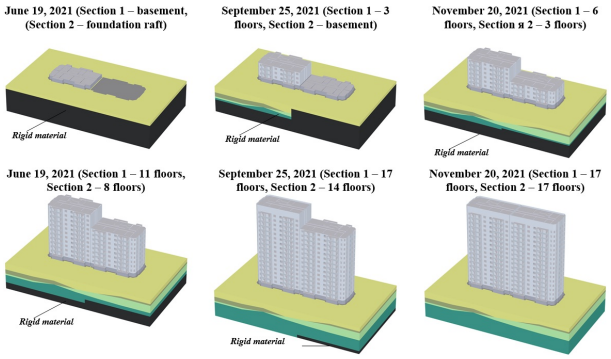

Figure 7. Calculation scheme of the model at the second stage of analysis with a stepped compressible layer based on observation dates and the number of erected floors.

Figure 8 presents a comparison of the calculated settlement values obtained for one of the simulation scenarios. The maximum and minimum settlement values are shown for both sections of the building, using the CSLFDC soil base model with either uniform or stepped compressible layer thicknesses under the foundations, corresponding to different construction stages with varying numbers of storeys.

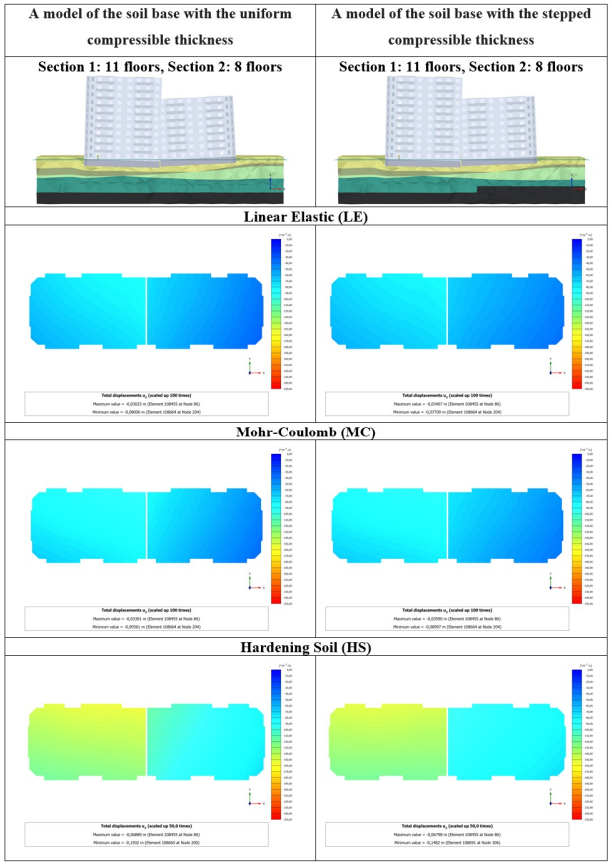

Figure 8. Comparison of calculation results for uniform and stepped compressible layer thicknesses as of 19.06.2021.

4 OBSERVATION RESULTS

Building settlements were monitored throughout the construction process using high-precision second-order leveling techniques. Settlement reference points M.1 through M.8 were established at the basement floor level of both sections of the structure (Figure 9).

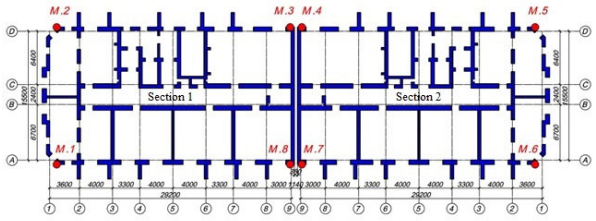

Figure 9. Settlement mark location diagram.

There were nine observation stages during the construction process. Leveling measurements were conducted using an H-05 level and an RN-05 invar leveling rod. The procedure involved combined forward and reverse runs. At each setup, height differences between the primary and auxiliary scales ($a_з$ and $a_п$) were recorded, and their difference $h = a_з - a_п$ was determined, not exceeding 0.7 mm. For each leveling segment between adjacent benchmarks, the total height differences were calculated for both the forward ($[h]_n$) and reverse ($[h]_з$) runs. The resulting discrepancies f_x remained within ±2.1 mm (where L is the segment length in kilometers) for sections with fewer than 15 setups.

Figure 10 presents graphs comparing the actual and calculated settlements of both sections of the building under monitored construction loads. Only the dead load from the erected structural elements was considered in the analysis, without the application of any load amplification factors.

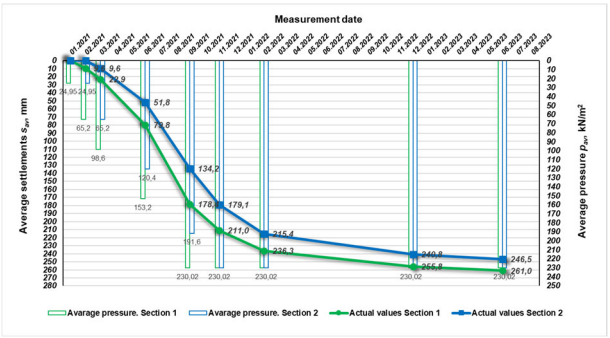

Figure 10. Average settlements of Sections 1 and 2 versus average pressure beneath the foundation slabs.

For improved clarity, Figure 11 and Figure 12 show a detailed comparison between measured and simulated settlement values based on the CSLFDC soil base model with a stepped compressible layer beneath the foundation slabs. The data correspond to the stage when both Sections 1 and 2 had reached 17 floors, with an average pressure beneath the foundations of $p_{av} = 230.02$ kN/m².

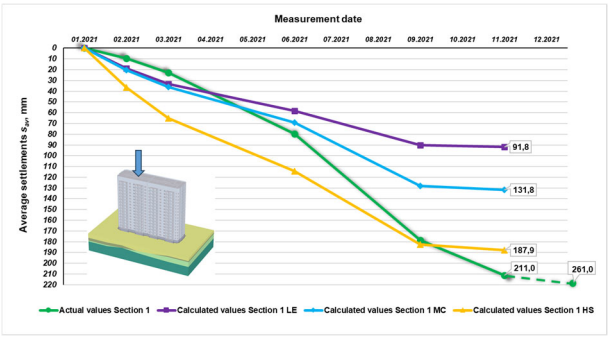

Figure 11. Average settlements of Section 1 compared to calculated values using the soil base model with a stepped compressible layer.

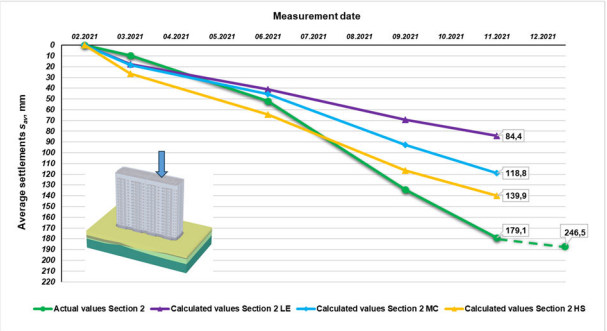

Figure 12. Average settlements of Section 2 compared to calculated values using the soil base model with a stepped compressible layer.

Figure 13 presents graphs of the actual and simulated horizontal displacements (tilts) of both building sections in the longitudinal direction, under monitored construction loads. As in previous analyses, only the dead load from the erected structural elements was considered, without applying any amplification factors.

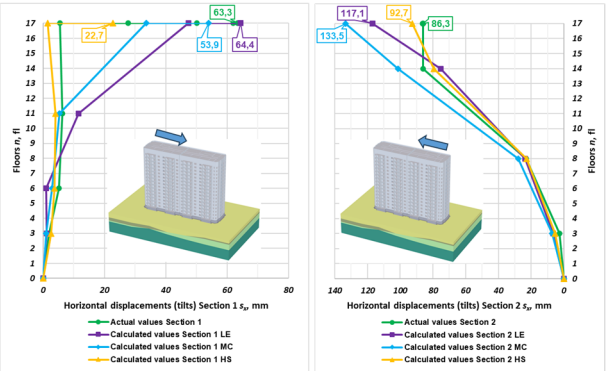

Figure 13. Horizontal movements (tilts) of Sections 1 and 2 along the longitudinal axis throughout the height compared to calculated values using the soil base model with a stepped compressible layer.

As shown in Figure 11 and Figure 12, the calculated settlement values that most closely matched the observed in-situ data were obtained using the Hardening Soil (HS) model. Nevertheless, the measured settlements exceeded the calculated ones by approximately 28% for Section 1 and 43% for Section 2. In comparison, deviations for the Linear Elastic (LE) and Mohr-Coulomb (MC) models were significantly higher - 65% and 50% for Section 1, and 66% and 52% for Section 2, respectively, in the downward direction.

The analysis of horizontal displacements (tilts) shown in Figure 13 indicates that, for Section 1, the most accurate match in absolute values was achieved using the Linear Elastic (LE) and Mohr-Coulomb (MC) models, with deviations of +2% (LE) and -15% (MC) relative to the measured values. However, the pattern of tilt development across the building height did not correspond to the observed behavior. In contrast, the Hardening Soil (HS) model most accurately reproduced the propagation trend of tilts at all stages of construction, despite an overall deviation of -64% from the measured magnitudes.

For Section 2, the differences between calculated and observed tilt values were +36% (LE), +55% (MC), and +7% (HS). It is important to note that the HS model parameters were applied in their default configuration within the Plaxis software, without additional calibration based on laboratory soil testing. Nevertheless, this approach provided the best agreement with the observed tilt propagation patterns for both sections, when using the soil base model in the form of a continuous layer of finite distribution capability with variable compressible thicknesses.

The convergence of tilts between the two building sections is consistent with classical theoretical solutions in continuum mechanics, specifically the principle of stress (strain) superposition under mutual structural interaction. However, as illustrated in Figure 13, the most pronounced interaction occurs at the final stage of construction, particularly when the vertical gap between the two sections does not exceed several floors (in this case, four). It is evident that the section constructed later - Section 2 - exerts a dominant influence on the overall deformation behavior of the system.

Figure 14 presents a general view of the completed building, including the expansion joint located at the interface between the two sections at the final stage of construction. The visual condition of the expansion joint indicates the absence of localized damage to the masonry on the upper floors, suggesting that no significant structural effects from “mutual loading” between the sections have occurred.

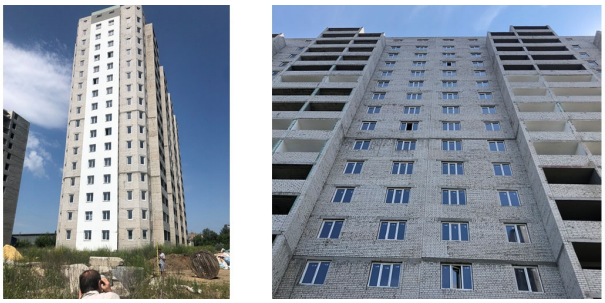

Figure 14. General view of the building and expansion joint at the final stage of construction.

5 CONCLUSIONS

The stress-strain behavior of the base – foundations - buildings system on large-area raft foundations was analyzed using PLAXIS soil models, confirming the applicability of the improved soil base model for adjacent buildings of differing storey heights.

The results of the research support the following conclusions and recommendations:

1. The effectiveness of the soil base model in the form of a continuous layer of finite distribution capability with variable compressible thicknesses, when used in combination with the elastoplastic Hardening Soil model, has been confirmed for predicting realistic deformations in sectional buildings on large raft foundations constructed over weak, water-saturated surface soils.
2. Comparative analysis of simulated and measured settlement and horizontal displacement (tilt) values for both sections demonstrates the suitability of the Hardening Soil model with stress-dependent stiffness for accurately reproducing observed behavior.
3. The analysis of measured tilt behavior in adjacent foundations of different-storey buildings shows that conventional continuous medium models with uniform compressible thickness do not adequately capture mutual structural interaction. This limitation is addressed through the use of the improved soil base model, which accounts for differentiated compressible layer thicknesses beneath each section in accordance with the applied loading.

6 REFERENCES

Braja M.D., 2017. *Shallow foundations. Bearing capacity and settlements*. CRC Press. Taylor & Francis Group.

Briaud, J-L., 2013. *Geotechnical Engineering: Unsaturated and Saturated Soils*. Hoboken, NJ: John Wiley & Sons, Inc.

DBN V.2.1-10:2018. Bases and foundations of buildings and structures. Main provisions. Kyiv: Ministry of Regions of Ukraine, State Enterprise Ukrarchbudinform. Ukrainian.

Empfehlungen des Arbeitskreises "Numerik in der Geotechnik" – EANG. *Deutsche Gesellschaft für Geotechnik e.V. (Ed.)*, 2014. German.

Kh Mohd Najmu Saquib Wani and Rakshanda Showkat, 2018. Soil Constitutive Models and Their Application in Geotechnical Engineering: A Review. *International Journal of Engineering Research & Technology (IJERT)*, 7(04), 137-145.

Kushner, S.G., 2008. *Calculation of deformations of the foundations of buildings and structures*. Zaporizhzhia. Russian.

Luchkovsky, I.Ya., 2000. *Interaction of structures with the soil base*. Kharkiv: KHDAKH (Library of the ITA journal), vol 3. Russian.

Lutchkovsky, I.J., and Samorodov, O.V., 2015. Definition of the parameters of an elastic finite layer. *Proceedings of the XVI European Conference on Soil Mechanics and Geotechnical Engineering for Infrastructure and Development*, Edinburgh, 3711-3715.

Nosenko, V.S., 2012. *Stress-strain state of plate-pile foundations of sectional high-rise buildings*. Doctoral dissertation, specialization 05.23.02. Kyiv: KNUBA. Ukrainian.

PLAXIS CONNECT Edition V20, 2020. *Material Models Manual*.

Samorodov A.V., 2017. *Design of high-performance combined pile-raft foundations for multi-story buildings: Monograph*. Kharkiv: Madrid Printing House. Russian.

Samorodov O. and Tabachnikov S., 2024. A Soil Base Model of Adjacent Various Story Structures. *Proceedings of 7th International Conference on Geotechnical and Geophysical Site Characterization.* Barcelona, Spain, 18-21 June 2024. Scipedia. Volume Field monitoring in geomechanics, 1144-1150. DOI: 10.23967/isc.2024.025

Samorodov, O.V. and Tabachnykov, S.V., 2023. Method for simulating a soil base of adjacent foundations [Sposib modeliuvannia hruntovoi osnovy poriad roztassovanykh fundamentiv] Ukraine Patent Application No. a202301804.

Samorodov, O.V., Alexandrovich, V.A., Tabachnykov, S.V., and Havryliuk, O.V., 2023. The influence of boundary conditions on the distribution capability and deformability of the soil base model with a linearly deformable, finite-depth soil layer. *Science and construction,* 2 (36), 12-19. Ukrainian.

Samorodov, O.V., Tabachnikov, S.V., Yesakova, S.V., and Krotov, O.V., 2024. Experience in Designing and Calculating Slab Foundations of a Two-Section Multi-story Building on Weak Water-Saturated Soils. In: Kolathayar, S., Vinod Chandra Menon, N., Sreekeshava, K.S. (eds). *Best Practices in Geotechnical and Pavement Engineering. IACESD 2023*. Lecture Notes in Civil Engineering, vol. 449. Springer, Singapore, 33–43.

Skochko, L., and Shabaltun, A., 2020. The influence of the sequence of building construction on the formation of the stress-strain state of the base-foundation-superstructures system. *Osnovu i fundamenty: Mizhvidomchyj naukovo-tekhnichnyj zbirnyk,* 41, 32-44. Ukrainian.

Ter-Martirosyan, Z.G., and Ter-Martirosyan, A.Z., 2009. Soil beds of high-rise buildings. *Soil Mechanics and Foundation Engineering*, 46(5), 165-179.

Vynnykov, Yu.L., 2005. *Modeling soil compaction processes in the axisymmetric stress-strain state of soil bases*. Doctoral dissertation, specialization 05.23.02. Kyiv. Ukrainian.